Testosterone signaling through ZIP9 renders melanoma more aggressive in males than in females

Cristina Aguirre-Portolés[1], Riley Payne[2], Aspen Trautz[1], J. Kevin Foskett[2], Christopher A. Natale[1], John T. Seykora[1], Todd W. Ridky[1]*

[1]Department of Dermatology, Perelman School of Medicine, University of Pennsylvania.
[2]Department of Physiology, Perelman School of Medicine, University of Pennsylvania, Philadelphia, PA. USA.
*Correspondence to: ridky@pennmedicine.upenn.edu

Abstract

Melanoma and most other cancers occur more frequently, and have worse prognosis, in males compared with females. Though sex steroids are thought to be involved, classical androgen and estrogen receptors are not detectable in most melanomas. Here we show that testosterone promotes melanoma proliferation by activating ZIP9 (*SLC39A9*), a zinc transporter that is not intentionally targeted by available therapeutics, but is widely expressed in human melanoma. This testosterone activity requires zinc influx, MAPK activation and YAP1 nuclear translocation. We demonstrate that FDA approved inhibitors of the classical androgen receptor also inhibit ZIP9, and thereby antagonize the pro-tumorigenic effects of testosterone in melanoma. In male mice, androgen receptor inhibitors suppressed growth of ZIP9-expressing melanomas, but had no effect on isogenic melanomas lacking ZIP9, nor on melanomas in females. These data suggest that ZIP9 might be effectively targeted in melanoma and other cancers by repurposing androgen receptor inhibitors that are currently approved only for prostate cancer.

Introduction

Cancer incidence and mortality are higher in males than in females in the U.S. and worldwide[1,2]. In the U.S., males are 15% more likely to develop cancer, and 40% more likely to die from this disease than females[1]. These sex differences were recognized as early as 1949[3], are observed in the majority of cancer types from non-reproductive tissues[1], and remain even after controlling for known risk factors such as environmental and occupational exposures[4]. While recent advances in modern targeted and immune therapeutics have markedly improved survival for both female and male melanoma patients[5], females still have more favorable outcomes[1,4]. Incidence and rate death for melanoma are 1.6X and 2.5X higher, respectively, in males than in females in the U.S[1]. Defining the mechanisms underlying the broad and persistent sex differences in cancer incidence and outcomes will address a major unresolved question in cancer pathobiology.

We previously showed that the female sex hormone estradiol inhibits melanoma proliferation and tumor growth *in vivo*. This effect is independent of biologic sex of the tumor, independent of classical estrogen receptors (ER), and results from activation of a nonclassical surface estrogen receptor on melanocytes and melanoma cells called the G Protein Estrogen Receptor (GPER)[6,7]. This work led us to consider whether male sex hormone signaling might also contribute to female vs. male differences in melanoma progression. Testosterone is the most abundant androgen and circulates at much higher levels in males (630 ng/dl) than in females (32 ng/dl)[8]. This androgen promotes proliferation *in vitro* in non-gonadal cell types including adipocytes[9], mouse skeletal muscle myoblasts[10], glioblastoma-derived cells[11], lung cancer cell lines[12] and melanoma[13]. As the classical androgen receptor (AR) is not consistently detected in most of these tissues, the receptor(s) mediating the testosterone-dependent proliferation increase and the corresponding downstream mechanisms are not yet defined. Also unknown is whether

53 this androgen activity observed *in vitro* is relevant to cancer progression *in vivo*. Here, we define
54 a nonclassical testosterone signaling pathway that establishes a novel mechanistic link between
55 male androgens and melanoma behavior, and highlights a new therapeutic opportunity using
56 currently-available drugs.
57

58 **Results**
59

60 **Melanoma tumors grow more quickly in male vs. female mice**
61
62 To test whether preclinical melanoma models recapitulate the male vs. female survival disparity
63 observed in humans, we first determined growth of human BRAF-driven melanoma (WM46,
64 female origin, $BRaf^{V600E}$; $CDK4^{R24C}$). Tumors grew faster in immunodeficient SCID male mice
65 compared with matched female mice (Fig. 1A and Fig. S1A), indicating that the differences do
66 not depend on T and/or B cell immune responses. To test whether this phenotype extends to a
67 genetically-engineered preclinical mouse model, we used murine YUMM1.7 cells (male origin,
68 $BRaf^{V600E/wt}$;$Pten^{-/-}$$CdkN2a^{-/-}$)[14] in syngeneic immunocompetent C57BL/6 mice. These tumors
69 also consistently grew faster in male mice compared with matched females (Fig. S1B).
70

71 **Testosterone, but not dihydrotestosterone, promotes proliferation in melanoma cells**
72 **independent of the classical androgen receptor**
73 Physiologic concentrations of testosterone promoted proliferation of both normal early passage
74 primary human melanocytes and melanoma cells (Fig. 1B, C and Fig. S1C). The proliferative
75 response to testosterone correlated to the dose and was saturable, suggesting a specific receptor-
76 mediated activity. In contrast, dihydrotestosterone (DHT) had no effect on proliferation of these
77 cell types across a wide concentration range (Fig. 1C).

78 Dihydrotestosterone is a more potent AR agonist than testosterone[15,16]. The fact that the
79 melanocytes and melanoma cells responded to testosterone, but not to DHT (Fig. 1B, 1C, Fig
80 S1D, E), suggests the possibility that a nonclassical androgen receptor mediates testosterone
81 effects in these cells. Supporting this idea, we were unable to detect AR mRNA transcript in any
82 of the 8 melanoma cell lines and primary primary melanocytes (MCs) we tested, although AR
83 mRNA was readily detectable in prostate cancer cells (Fig. 1D and Fig. S1F). Consistent with
84 this lack of AR transcript, we were also unable to detect clear AR protein in these cells via
85 western blotting using 2 different AR antibodies, or via immunofluorescence directly on the
86 cultured cells, although AR protein was readily detectable in 2 prostate cancer lines used as
87 positive controls (Fig. 1E and Fig. S1G). A faint signal suggestive of AR was seen on the
88 western blot and IF from a single cell line (A375) using a single antibody (EPR1535). However,
89 the identity of this weak signal is not clear, as it was not seen with the other antibody (D6F11),
90 and qPCR did not show any significant AR transcript.

91 To begin testing whether a nonclassical androgen receptor mediates testosterone effects
92 in melanoma we looked to *SLC39A9*/ZIP9, a transmembrane zinc transporter recently discovered
93 in Atlantic Croaker (fish) cells to be a activated by androgen, and unlike AR, to have much
94 higher affinity for testosterone than for dihydroteststerone[17]. ZIP9 transports zinc (Zn^{++}) across
95 cell and organelle membranes into the cytoplasm and is the only steroid receptor known to
96 directly regulate zinc homeostasis[18]. The human ZIP9 homolog, encoded by the *SLC39A9* gene,
97 is broadly expressed in most cancers (Fig. S2A), normal human melanocytes, and all melanoma
98 lines that we tested (Fig. 2A). To test whether ZIP9 was active in melanoma we used the
99 fluorescent Zn^{++}-specific probe FluoZin-3. Testosterone induced a rapid increase in cytosolic
100 free Zn^{++} ($[Zn^{++}]_i$) in human melanoma cells (Fig. 2B), that was followed by a sustained

101 elevation for at least 2 days in the presence of the testosterone (Fig. 2C). We determined that
102 Zn^{++} influx was necessary for the testosterone-dependent increase in melanoma cell proliferation,
103 as treatment with the Zn^{++} chelator N,N,N′,N′-tetrakis (2-pyridinylmethyl)-1,2-ethanediamine
104 (TPEN), blocked testosterone induced proliferation at TPEN concentrations that had no
105 significant effect on proliferation when used alone (Fig. 2D and Fig. S2B).

106 Although TPEN has high affinity for Zn^{++}, it also has some ability to chelate copper[19]. To
107 test whether copper flux might contribute to testosterone effects on melanoma proliferation, we
108 treated WM46 cells with $CuSO_4$, which had no significant effect on cell proliferation (Fig. S2C).
109 Moreover, the highly specific copper chelator bathocuproinedisulfonic acid (BCS), did not affect
110 the proliferative response to testosterone, nor did BCS affect testosterone induced Zn^{++} influx
111 (Fig. S2D and Fig. S2E).

112 After determining that Zn^{++} influx was necessary for testosterone-induced proliferation,
113 we next tested whether increased Zn^{++} was sufficient to increase melanoma proliferation.
114 Exogenous zinc pyrithione (also a Zn^{++} ionophore), and $ZnCl_2$ each increased melanoma
115 proliferation (Fig. 2E). Other biologically-relevant divalent cations, Fe^{++} and Mn^{++}, known to be
116 transported by other ZIP family members[20], had no effect on proliferation (Fig. 2E).

117 Together, these results demonstrate that testosterone, but not DHT, promotes zinc
118 dependent proliferation in melanoma cells that express ZIP9 and lack detectable AR.

119 We next used immunocytochemistry to test whether AR and/or ZIP9 protein are
120 expressed in human melanocytic lesions (14 benign nevi, 63 primary melanomas, and 21
121 metastatic melanomas).

122 AR was determined in tissue sections using the highly controlled CLIA (Clinical
123 Laboratory Improvement Amendments) certified method in the clinical pathology lab at the

124 Hospital of the University of Pennsylvania. This procedure uses a validated antibody different
125 from the two we used for western blotting and immunofluorescence. Each tissue was scored in a
126 blinded fashion by a board-certified pathologist. While AR was readily detectable in prostate
127 tissue used as positive control, AR was not detected in any of the nevi, nor in the melanomas
128 (Fig. 2F). In parallel, we analyzed the same samples for ZIP9. CLIA grade ZIP9 IHC is not
129 available. However, we validated our ZIP9 antibody using parental WM46 ZIP9 positive
130 (wtZIP9) and isogenic ZIP9 negative (ΔZIP9) isogenic cell lines. These cells were grown on
131 chamber slides and processed for IHC in parallel with the human samples. The antibody used
132 labeled only the wtZIP9 cells. ZIP9 protein was observed in 100% of the nevi, 97% of primary
133 melanomas and 100% of the metastatic samples (Fig. 2G). Further, ZIP9 relative staining
134 intensity positively correlated with tumor stage (Fig. 2H). No significant differences in ZIP9
135 staining were observed between males and females (Fig. S3).
136
137 **Testosterone signaling through ZIP9 promotes melanoma growth *in vivo***
138 To determine whether ZIP9 mediates testosterone effects in our models, we used CRISPR-Cas9
139 and gRNA targeting Slc39A9 exon1 to ablate ZIP9 in human (WM46) melanoma and murine
140 (YUMM1.7) melanoma. Isogenic clonal populations of parental ZIP9-expressing (wtZIP9) and
141 ZIP9-ablated (ΔZIP9) cells were established, and the mutations disrupting the reading frame
142 were mapped by sequencing (Fig. S4A, S4B and S4C). ZIP9 protein was not detectable in ΔZIP9
143 cells (Fig. 2F, Fig. 3A and Fig. S4D). ΔZIP9 cells did not respond to testosterone, whereas
144 isogenic wtZIP9 control clones responded similarly to the parental wtZIP9 cells (Fig. 3A and
145 Fig. S4E).

146 The testosterone insensitive phenotype associated with CRISPR-Cas9 engineered ZIP9 loss
147 was rescued by expression of a human ZIP9 transgene. Lentiviral mediated constitutive ZIP9
148 expression in the ΔZIP9 WM46 cells restored both ZIP9 protein and the proliferative response to
149 testosterone (Fig. S4F, S4G).

150 Consistent with the conclusion that ZIP9 is the major mediator of testosterone and
151 exogenous zinc effects in these melanoma cells, exposure to testosterone or to extracellular zinc
152 failed to increase $[Zn^{++}]_i$ in ΔZIP9 cells (Fig. 3B and 3C). Therefore, testosterone induces a rapid,
153 ZIP9-dependent, increase in $[Zn^{++}]_i$ that is required for the increased proliferation in melanoma
154 cells.

155 We next used the ΔZIP9 cells to test whether ZIP9 influences melanoma progression *in*
156 *vivo.* We subcutaneously injected WM46 wild-type and isogenic ΔZIP9 WM46 cells into the
157 flanks of SCID mice. Melanomas with complete ZIP9 ablation grew more slowly in both male
158 and female mice, suggesting that while ZIP9 is stimulated by testosterone, ZIP9 has some basal
159 Zn^{++} transport activity, and/or other functions that help maintain cell fitness (Fig. 3D and Fig.
160 S4H). However, the effects of ZIP9 loss on tumor growth were greatest in males. In parental wt
161 tumors, male sex appears to promote both the early and later stages of tumor progression (Fig.
162 1A). In model melanomas lacking ZIP9, which seems not to occur in spontaneous human
163 melanoma, male sex preferentially promotes the earlier stages of tumor growth (Fig. 3D).
164 wtZIP9 tumors were consistently much bigger in males, and this difference was already evident
165 by day 6. Exponential curve fit analysis in this experiment shows that subsequent tumor
166 doubling times are similar between the groups (Fig. S4I).

167 Together these data indicate that ZIP9 activity promotes melanoma, and suggests that
168 ZIP9 is a determinant of the male vs. female differences in these preclinical tumor models.

169 **Testosterone-induced melanoma proliferation through ZIP9 requires downstream MAPK**
170 **and YAP1 activation**

171 Although the studies detailed above show that testosterone promotes melanoma proliferation via
172 ZIP9 dependent Zn^{++} influx, zinc is involved in myriad cellular processes, making it difficult to
173 predict *a priori* which downstream signaling pathways are required for the testosterone activity.
174 To start identifying these, we used a 447-element Reverse Phase Protein Array (RPPA) analysis
175 of human WM46 melanoma cells treated with testosterone for 0, 30, 60 and 480 min. While the
176 relative expression of most represented proteins was unaffected by testosterone, some were
177 significantly under or overexpressed, including several with known tumor-promoting or tumor-
178 suppressive functions (Fig. 4A and Table S1).

179 Downregulated proteins included 14-3-3ε, a tumor suppressor and negative YAP1
180 regulator previously implicated in liver, lung, and gastric cancers[21], and CDKN2A (p16), a
181 cyclin-dependent kinase (CDK) inhibitor, and one of the most studied tumor suppressors[22].
182 Upregulated proteins included key elements of tumor-promoting pathways, most notably
183 phosphorylated ERK (T202; Y204) and YAP1 (Fig. 4A). Importantly, ΔZIP9 cells displayed
184 decreased basal levels of ERK phosphorylation compared with isogenic wild-type clones (Fig.
185 S5A). MAPK activation was necessary for the testosterone-dependent proliferative response, as
186 the specific ATP-competitive ERK1/2 inhibitor, ulixertinib[23] (RVD-523) blocked the
187 testosterone-dependent proliferative response, at ulixertinib concentrations that had no effect on
188 the basal proliferation rate when used alone (Fig. 4B).

189 Testosterone-dependent ZIP9 activation appeared to render WM46 cells more sensitive to
190 ulixertinib, as cell viability was compromised when they were treated with both compounds.
191 This vulnerability to combination treatment seems to be specific and ZIP9 dependent, as ΔZIP9

192 cells treated with both testosterone and ulixertinib proliferated at rates comparable to controls
193 (Fig. 4B).

194 We determined that YAP1 activation is also required for the augmented proliferative
195 response driven by testosterone. YAP1 is a transcriptional coactivator whose activity is largely
196 regulated by its localization[24]. Testosterone induced rapid YAP1 translocation from cytoplasm to
197 nucleus in human melanoma cells in a ZIP9-dependent manner (Fig. 4C, 4D and Fig. S5B).
198 YAP1 subcellular localization is controlled largely by LATS, which phosphorylates YAP1 at
199 Serine 127 and thereby retains YAP1 in the cytoplasm[25]. The YAP1 inhibitor dobutamine also
200 promotes phosphorylation of YAP at Ser127[26]. Consistent with this, the testosterone induced
201 YAP1 nuclear localization and increase in cell proliferation were both blocked by dobutamine,
202 while dobutamine had no significant effect on its own (Fig. 4D, Fig. S5C and Fig. 4E). When
203 ZIP9 expression was rescued via lentiviral transduction of a ZIP9 transgene to ΔZIP9 WM46
204 cells, testosterone dependent YAP1 translocation into the nucleus was restored (Fig. S5C).

205 Testosterone promotion of YAP1 activity was evidenced by increased expression of
206 several well-known YAP1 target genes including CDC6, CTGF, CYR61 and THBS1. As
207 expected, these testosterone-induced expression changes were also blocked by dobutamine (Fig.
208 4F).

209

210 **Pharmacologic ZIP9 blockade inhibits testosterone-driven melanoma proliferation and**
211 **melanoma tumor growth *in vivo.***

212 We next tested whether FDA-approved compounds could be repurposed to effectively
213 target ZIP9. Although specific ZIP9 inhibitors are not yet developed, molecular modeling and
214 competition assays with fluorescent-tagged testosterone suggest that the androgen receptor

215 inhibitor bicalutamide (BIC) competes with testosterone for ZIP9 binding to the same
216 extracellular pocket and thereby acts as a competitive ZIP9 antagonist[27]. Bicalutamide was
217 developed and approved for prostate cancer and has now been largely replaced by enzalutamide
218 (ENZ) and apalutamide (APA), which are structurally related analogs with higher affinity for the
219 androgen receptor and greater clinical efficacy against advanced prostate cancer[28,29].

220 While ZIP9 was not known to be an androgen receptor at the time these drugs were
221 developed, we show here that they are nonetheless effective inhibitors of testosterone effects in
222 melanoma cells that lack detectable AR, but that do express ZIP9. Each compound completely
223 blocked testosterone-induced proliferation and MAPK activation in several melanoma cell lines
224 (Fig. 5A, 5B). Importantly, these agents alone (without testosterone) had no effect on cell
225 proliferation (Fig. S6A). The testosterone dependent increase of intracellular zinc was also
226 efficiently blocked by bicalutamide (Fig. S6B). Moreover, ΔZIP9 cells transduced to re-express
227 ZIP9, responded to testosterone, and this effect was again blocked by bicalutamide (Fig. S6C).

228 To further confirm that these pharmacologic agents work through ZIP9, we next used
229 cyproterone acetate (CPA), an anti-androgen that blocks the testosterone interaction with AR, but
230 that does not bind to ZIP9[30]. In our melanoma cells, up to a 20-fold molar excess of CPA did not
231 significantly inhibit testosterone effects on proliferation, consistent with the conclusion that AR
232 is not the major mediator of testosterone effects in these melanoma models (Fig. S6D).

233 To test whether these pharmacologic flutamide class AR inhibitors block the physical
234 interaction between testosterone and ZIP9 in melanoma, we performed direct binding assays
235 using a membrane-impermeable testosterone analogue (T-BSA-FITC). This reagent labels the
236 plasma membrane surface of wild-type ZIP9 expressing WM46 melanoma cells (Fig. 5C). This
237 membrane bound testosterone was displaced by apalutamide, demonstrating the specificity of the

238 interaction. Further demonstrating that the binding is ZIP9 specific, testosterone localization at
239 the plasma membrane was markedly reduced in ΔZIP9 cells (Fig. 5C) and was unaffected by
240 apalutamide (Fig. 5D).

241 Next, we tested whether apalutamide and related analogs inhibit melanoma *in vivo*. For
242 this, we introduced wtZIP9 or isogenic ΔZIP9 human WM46 melanoma into SCID mice. Once-
243 daily systemically administered apalutamide (20 mg/kg/day via oral gavage) significantly
244 suppressed growth of wtZIP9 tumors in male mice and extended its survival (doubling time for
245 tumor growth was 11.1 days for vehicle treated males and 25.2 days for APA treated males) (Fig.
246 5E, Fig. S7A). Similar results were obtained when males were treated with bicalutamide
247 (30mg/kg/day) (Fig. S7B). Importantly, bicalutamide had no effect on wtZIP9 tumors in female
248 mice, nor on ΔZIP9 tumors (Fig. S7C). Together, these data show that nonclassical androgen
249 signaling through ZIP9 promotes melanoma progression specifically in males.

250

251 **Discussion**

252

253 Although many have speculated that sex steroids contribute to sex differences in cancer
254 pathobiology, definitive functional studies are lacking, and the mechanisms by which they
255 contribute to the male-female cancer sex gap are largely unknown. We previously described the
256 tumor suppressor activity of the nonclassical estrogen receptor GPER in melanoma[6]. This
257 finding led us to question whether circulating androgens in males might also contribute to the
258 melanoma sex gap.

259 Testosterone promoted proliferation of melanoma cells in a saturable-dose-dependent
260 manner. Curiously, the same cell lines did not respond to DHT, which is generally considered
261 the more biologically active androgen. DHT displays 4-fold increased affinity than testosterone

262 for AR, and it dissociates from AR three time slower than testosterone[16]. Lack of response to
263 DHT in melanoma is consistent with the absence of detectable AR expression in the models used
264 for this study, and is highly consistent with our genetic data showing that ZIP9, which has higher
265 affinity for testosterone vs. DHT, is an important mediator of testosterone effects.

266 The effects of testosterone signaling through ZIP9 in cancer cells may vary with cancer
267 type. Testosterone has been shown to induce apoptosis in some prostate cancer cells (PC-3) via
268 Bax up-regulation[31,32]. In our cultures of melanocytes and melanoma cells +/- testosterone, we
269 did not observe any obvious cell death, and testosterone increases cell numbers, rather than
270 decreases them. In a comprehensive RPPA analysis of protein expression in human melanoma
271 cells treated with testosterone (Figure 4A), no significant differences were found in any of 8
272 major pro- and anti-apoptotic regulators (Bax, Bad, Bak, Bim, Bcl-2, Bcl-xL, Bcl-2A1, Mcl-1)
273 (Fig. S8). It therefore appears unlikely that apoptosis significantly affects the testosterone driven
274 phenotype we observe in melanoma.

275 We show here that ZIP9 activation, via testosterone binding, promotes an increase in
276 cytosolic zinc in melanoma cells. The mammalian family of zinc transporters SLC39A
277 comprises 14 members (ZIP1–14)[33] grouped into four subfamilies that were stablished according
278 to their amino acid sequence similarities. There may be roles for these other family members in
279 some cancers, as ZIP1 (SLC39A1, from ZIPII subfamily), has been associated with the
280 regulation of zinc uptake in prostate cancer cells[34]. However, this rapid increase of intracellular
281 zinc through ZIP1 appears to be AR dependent, as PC-3 cells only respond to testosterone after
282 they are transfected with exogenous AR. ZIP9 amino acid residues predicted to be most critical
283 for testosterone and bicalutamide binding include Ala167, Val241, Met248, and Ala167, Leu302,
284 Ser171, respectively[27], however only Ala167 is present in ZIP1, suggesting that this receptor

285 may not be similarly regulated by testosterone. Regarding other members of the SLC39A family,
286 ZIP9 is unique member of ZIPI subfamily[35], and the only one known to directly interact with
287 testosterone.

288 A recent report[36] published while this manuscript was in revision also considered a
289 possible role for testosterone in melanoma and concluded that the androgen promotes melanoma.
290 Authors attributed this effect to the classical AR. However, that report did not consider ZIP9, did
291 not show that AR was necessary for melanoma response to pharmacologic AR inhibitors, and did
292 not show that AR was a determinant of sex differences in melanoma tumor growth. Here we
293 studied 98 human melanocytic lesions (nevus, primary and metastatic melanoma) and did not
294 detect AR in any of them, while ZIP9 protein was detectable in 97% and 100% of the primary
295 and metastatic melanomas respectively. We recognize the possibility that some melanoma cell
296 lines in use by other laboratories, and perhaps even some human tumors, may express AR that
297 contributes to melanoma growth, but these are likely rare compared to melanomas that are
298 affected by ZIP9.

299 There may be many drivers of the cancer sex gap in humans, including differences in
300 immune surveillance[37]. However, differences in immune surveillance do not appear to be a major
301 driver of the differences in the melanoma models used for this study, as tumors progressed faster
302 not only in male vs. female immunocompetent mice, but also in human melanomas grown in
303 male vs. female SCID mice. Therefore, the testosterone effects on melanoma in these models are
304 dependent on ZIP9, but independent of B and T cell mediated anti-tumor activity. Consistent
305 with this, ZIP9 expressing tumors respond to bicalutamide and apalutamide in SCID mice, and
306 genetic ZIP9 depletion collapsed the sex gap.

307 As ZIP9 is widely expressed in nearly all tissues, it may be a major determinant of the
308 sex disparity in outcomes not just for melanoma, but also for many other cancer types.
309 Consistent with this, we observed that testosterone promotes proliferation in many diverse cancer
310 cell types, and that this effect is blocked by bicalutamide (Fig. S9). The demonstration here that
311 ZIP9 is pharmacologically accessible, suggests that ZIP9 may be a new eminently druggable
312 therapeutic target (Fig. 5F), and that currently approved androgen receptor inhibitors might be
313 useful alone, or in combination with current standard of care therapeutics for a wide range of
314 cancers, especially those that disproportionately affect males.
315

316 **Materials and Methods**
317

318 **CRISPR-Cas9 mediated ablation of Slc39A9**

319 We used lentiviral transduction to deliver dox-inducible Cas9 and gRNA targeting exon 1 of
320 Slc39A9 in human WM46 and murine YUMM1.7 melanoma cells. Transduced cells were
321 selected with puromycin, and single cells subsequently isolated, expanded and examined for
322 ZIP9 protein expression, compared to clones isolated in parallel with no doxycycline treatment.
323 The following gRNA sequences were used (5'-3'):
324 hZIP9_gRNA_Fw caccgTTGGTGGGATGTTACGTGGC
325 hZIP9_gRNA_Rv aaacGCCACGTAACATCCCACCAAC
326 hZIP9_gRNA_Fw caccgCGTGGCCGGAATCATTCC
327 hZIP9_gRNA_Rv aaacGGAATGATTCCGGCCACG
328 To map the targeted sequencing, the region surrounding the gRNA target sequence was
329 amplified in both WM46 (282bp) and YUMM1.7 (259bp) isogenic clones. The following

330 primers were used (5'-3'): hZIP9_CRISPRmut_Fw:
331 TAAGCAGAATTCATGGATGATTTCATCTCC
332 hZIP9_CRISPRmut_Rv:TAAGTAAGTCCAAGCTTCTGCTGCTTTGTCTGATGCA.
333 mZIP9_CRISPRmut_F:TAAGCAGAATTCATGGATGACTTTCTCTC.
334 mZIP9_CRISPRmut_Rv TAAGTAAGTCCAAGCTTGATATTTCTGCTGCTTTGT.
335 Once amplified, DNA fragments were cloned into pUC19 vector using EcoRI and HindDIII
336 sites, and sequenced (Sanger) by the DNA Sequencing Facility (University of Pennsylvania).
337 Sequences were analyzed using the free software CRISP-ID (V1.1) and ICE Analysis by
338 Synthego were the knock-out scores were obtained.
339

340 **Cell culture and proliferation assays**

341 YUMM1.7, SH-4 and SK-MEL-2 cells were purchased from ATCC (YUMM1.7 ATCC® CRL-
342 3362™; SH-4 ATCC® CRL-7724™; SK-MEL-2 ATCC® HTB-68™) and cultured in DMEM
343 (Mediatech, Manassas, VA, USA) with 5% FBS (Invitrogen, Carlsbad, CA, USA) and 1%
344 Penicillin-Streptomycin (Thermo Fisher Scientific. # 15140122). SK-MEL-3 cells were
345 purchased from ATCC (ATCC® HTB-69™ and cultured in McCoy's 5A (Modified) Medium
346 with 10% FBS (Invitrogen, Carlsbad, CA, USA) and 1% Penicillin-Streptomycin. SK-MEL-24
347 cells were purchased from ATCC (ATCC® HTB-71™) and cultured in Eagle's Minimum
348 Essential Medium with 15% FBS and 1% Penicillin-Streptomycin. WM46 melanoma cells were
349 a gift from Meenhard Herlyn (Wistar Institute, Philadelphia, PA, USA) and were cultured in
350 TU2% media. Tumor cells were regularly tested using MycoAlert Mycoplasma Detection Kit
351 from Lonza (Allendale, NJ, USA). For monitoring cell proliferation $10x10^5$ YUMM1.7 or
352 $12x10^5$ WM46 cells were seed per well in 12-well Cell culture Plates. All the experiments

353 performed in this work utilized charcoal stripped serum (Fetal Bovine Serum, charcoal stripped,
354 USDA-approved regions, One Shot™ format. Catalogue number #A3382101; Thermofisher
355 Scientific). Cells were treated every second day and manually counted in triplicate using a
356 hemocytometer. All the experiments were performed in cell populations that were in culture
357 during a maximum of 3 weeks (5 passages in average) since thaw from the corresponding stock.
358

359 **Zinc influx analysis**

360 WM46 cells were loaded with 5 µM FluoZin™-3, AM cell permeant™ (Thermo Fisher
361 Scientific, #F24195), for 20 minutes then incubated in 2 Ca Tyrode's solution (in mM: 140
362 NaCl, 5 KCl, 1 $MgCl_2$, 2 $CaCl_2$, 10 glucose and 5 (Na) Pyruvate – pH 7.4) for 5-10 minutes at
363 room temperature prior to imaging. Cells were imaged on a Nikon Ti microscope using a
364 20x/0.75 NA objective for fluorescence at 340 nm and 380nm excitation/515 nm emission (Ca^{2+}-
365 free Fura2 or FluoZin™-3) and 380 nm excitation/515 nm emission (Ca^{2+}-free Fura2 FluoZin™-
366 3). Coverslips were perfused at 1-3 mL/min following this protocol: Ca^{2+} Tyrode's (0-30 secs);
367 Ca^{2+} Tyrode's + DMSO & 5 uM Zinc (30-90 secs); Ca^{2+} Tyrode's + Testosterone & 5□M Zinc
368 (90-360 secs); Ca^{2+} Tyrode's + Testosterone + BIC & 5 uM Zn (360-470 secs); Ca^{2+} Tyrode's
369 washout (470-500 secs). 100 milliseconds exposure images for each wavelength were collected
370 every 2 seconds. For analyzing the long-term consequences of testosterone treatment, cells were
371 treated with the androgen for 96 hours and then loaded FluoZin™-3. Cells were incubated with
372 FluoZin™-3 following manufacturer recommendation and exposed to 400nM Zn pyrithione or
373 $ZnCl_2$. Images were acquired with EVOS BLA. Fluorescence was quantitated using ImageJ
374 (National Institutes of Health, Bethesda, MD, USA), and statistical analyses were performed
375 using Graphpad Prism software.

376 **Reverse Phase Protein Array (RPPA)**

377 We used the Functional Proteomics Core at MD Anderson
378 (https://www.mdanderson.org/research/research-resources/core-facilities/functional-proteomics-
379 rppa-core.html) to perform a 447-element Reverse Phase Protein Array (RPPA) analysis of
380 human melanoma cells grown in medium with stripped serum and treated with testosterone
381 (100nM) for 0, 30', 60' and 8 hours. Cells were tripsinized and washed with PBS. After
382 centrifugation (5 minutes; 1200rpm), supernatant was discarded, and cells were frozen at -80ºC
383 prior to be sent to the Functional Proteomics Core at MD Anderson.

384

385 **Western blot, immunofluorescence and antibodies**

386 Adherent cells were washed once with PBS and lysed with 8M urea containing 50mM NaCl and
387 50mM Tris-HCl, pH 8.3, 10mM dithiothreitol, 50mM iodoacetamide. Lysates were quantified
388 (Bradford assay), normalized, reduced, and resolved by SDS gel electrophoresis on 4–15%
389 Tris/Glycine gels (Bio-Rad, Hercules, CA, USA). Resolved protein was transferred to PVDF
390 membranes (Millipore, Billerica, MA, USA) using a Semi-Dry Transfer Cell (Bio-Rad), blocked
391 in 5% BSA in TBS-T and probed with primary antibodies recognizing β-actin (Cell Signaling
392 Technology, #3700. 1:4000, Danvers, MA, USA), ZIP9 (Abcam, #137205, 1:500), P-ERK (Cell
393 Signaling Technology, Phospho-p44/42 MAPK (Erk1/2) (Thr202/Tyr204) (D13.14.4E) XP®
394 Rabbit mAb #4370. 1:1000), ERK (Cell Signaling Technology, p44/42 MAPK (Erk1/2) (137F5)
395 Rabbit mAb #4695, 1:1000), Androgen Receptor [(D6F11) XP® Rabbit mAb #5153] and
396 Recombinant Anti-Androgen Receptor antibody [EPR1535(2)] (ab133273. Antibody already
397 validated by the Human Protein Atlas). After incubation with the appropriate secondary antibody
398 [(Rabbit Anti-Mouse IgG H&L (Biotin) preabsoFS9rbed (ab7074); Anti-mouse IgG, HRP-linked

399 Antibody #7076. 1:2000)] proteins were detected using ClarityTM Western ECL Substrate (Bio-
400 Rad. #170-5060). All western blots were repeated at least 3 times. To monitor YAP1 nuclear
401 translocation by western blot analysis, nuclear fractionation was performed using protein lysis
402 buffer containing 10mM HEPES, 1mM KCl, 1.5mM MgCl2 and 10% glycerol (Buffer A). After
403 washing the adherent cells with DPBS, samples were resuspended in Buffer A and incubated for
404 5 minutes on ice in the presence of 0.1% Triton-X-100. After centrifugation, the nuclear fraction
405 remained as a pellet while the supernatant corresponding to the cytosolic fraction. Nuclear
406 fraction was washed with Buffer A. After centrifugation, the nuclear fraction was resuspended in
407 RIPA buffer and samples were boiled for 5 min prior to sample loading. The cytosolic fraction
408 was centrifuged for 15 min at 13500 rpm. Only the supernatant was kept after centrifugation.
409 Western blot was performed as described before and the following antibodies were used for
410 protein detection: β-tubulin (Cell Signaling Technology, β-Tubulin (9F3) Rabbit mAb #2128.
411 1:1000), PARP (Cell Signaling Technology, Rabbit mAb #9542. 1:1000), YAP1 (Cell Signaling
412 Technology, YAP (D8H1X) XP® Rabbit mAb #14074. 1:1000). For immunofluorescence in
413 adherent cells, samples were fixed with 4% paraformaldehyde (Affymetrix; #19943) for 7 min at
414 room temperature and permeabilized with iced-cold methanol. After blocking with 10%
415 FBS:0.03%Triton-X100, primary antibodies were incubated overnight in blocking solution (β-
416 actin and YAP1 antibodies detailed above). After three washes in DPBS:0.03% Triton X-100)
417 cells were incubated with secondary antibodies for 45 minutes at room temperature [(Goat anti-
418 Mouse IgG (H+L) Highly Cross-Adsorbed Secondary Antibody, Alexa Fluor 594. Goat anti-
419 Rabbit IgG (H+L) Highly Cross-Adsorbed Secondary Antibody, Alexa Fluor 488)]. Cells were
420 rinsed with PBS-0.03%-Triton three times and coverslips were mounted with ProLong Gold
421 antifade reagent with DAPI (#P36935; Thermo Fisher Scientific). Images were captured using a

422 Leica DM IL microscope and registered using LAS software. For fluorescence intensity
423 quantification ImageJ software (National Institutes of Health, Bethesda, MD, USA) was used,
424 and statistical analyses were performed with GraphPad Prism software.
425
426 **Immunohistochemistry and quantification**
427 FFPE tissue microarrays (ME1004h: Malignant melanoma, metastatic malignant melanoma and
428 nevus tissue array) were obtained from US Biomax, Inc. (Derwood, MD). For the staining with
429 anti-ZIP9 antibody [(SLC39A9 Antibody (PA5-52485), Thermofisher Scientific, Waltham,
430 MA)], slides were deparaffinized and rehydrated following the standard immunohistochemistry
431 protocol [(xylenes 5 minutes x 3, 100% alcohol (5 min. x 3), 95% alcohol (5 min.), 80% alcohol
432 (5 min.), 70% alcohol (5 min.), and 50% alcohol (5 min.) and finished with distilled water)]. The
433 antigen retrieval was done by loading the slides into a retriever (Electron Microscopy Sciences
434 EMS) with R-Buffer A. After 20 minutes, samples were allowed to cool for 30 minutes inside
435 the retriever and for 20 minutes at room temperature. Samples were washed twice with PBS and
436 blocked with Dako Dual Endogenous Enzyme Block (Code S2003. Agilent Santa Clara, CA) for
437 20 minutes at R.T. Samples were washed twice with PBS and blocked for 20 minutes with 2
438 drops of Vector Avidin Block. After washing twice with PBS, slides were blocked for 20
439 minutes with two drops of Vector Biotin Block (Avidin/Biotin Blocking kit. SP-2001. Vector
440 Laboratories, Inc. Burlingame, CA). Samples were washed twice with PBS with Protein Block
441 Serum-Free Ready-To-Use for 30 minutes at R.T. (Code X0909. Agilent Santa Clara, CA).
442 Primary antibody was prepared 1:500 in PBST (100µl per slide) and samples were incubated
443 overnight at 4°C. Samples were washed three times with PBS and incubated with Biotinylated
444 Secondary antibody (Vectastain Kit, Peroxidase Rabbit IgG, PK-4001) for one hour at R.T. After

445 three washes with PBS, ABC reagent (prepared 30 minutes in advance) was added and samples
446 were incubated for 30 minutes at R.T. Samples were washed twice with PBS and incubated for 3
447 minutes with ImmPACT® DAB Substrate, Peroxidase (HRP) (SK-4105. Vector laboratories,
448 Burlingame, CA). Tissues were counterstained with hematoxylin (30 seconds, R.T.) (GHS316.
449 Sigma-Aldrich) dehydrated, and mounted with SecureMount (Fisher HealthCare™
450 PROTOCOL™ Mounting Media. #022-208. Fisher Scientific. Thermofisher Scientific). John T.
451 Seykora M.D., Ph.D, performed scoring of the stained tissue microarray, and scoring index was
452 determined by scoring the percentage of positive cells on a scale of 0 to 3 as well as the intensity
453 of ZIP9 staining on a scale of 0 to 4 (1=1-25%, 2=26-50%, 3=51-75%, 4=76-100%).
454 The staining of the tissue microarrays (ME1004h) for AR detection was performed by
455 University of Pennsylvania Pathology Clinical Service Center—Anatomic Pathology Division,
456 using the highest grade, CLIA (Clinical Laboratory Improvement Amendments) certified and
457 validated test available. Briefly, five-micron sections of formalin-fixed paraffin-embedded tissue
458 were stained using antibody against Androgen Receptor [(Leica AR-318-L-CE, clone AR27
459 (clone AR27, 1:25)]. Staining was done on a Leica Bond-IIITM instrument using the Bond
460 Polymer Refine Detection System (Leica Microsystems DS9800). Heat-induced epitope retrieval
461 was done for 20 minutes with ER2 solution (Leica Microsystems AR9640). All the experiment
462 was done at room temperature. Slides are washed three times between each step with bond wash
463 buffer or water. The slides were reviewed and scored in blinded fashion by a board-certified U.
464 Penn pathologist. Prostate tissue was used as the positive control.
465
466
467

468 **Immunocytochemistry**

469 To detect ZIP9 protein in WM46 isogenic clones, the protocol described in ProSciΨ™ for
470 immunocytochemistry. Briefly, cells were fixed in 4% PFA for 7 minutes. After two washes with
471 PBS (5min), cells were permeabilized with PBS/0.1% Triton X-100 for 1 minute at R.T. Cells
472 were washed twice with PBS on a shaker. Once treated with 1.5% H_2O_2/PBS solution for 15
473 minutes (R.T.), cells were washed again and blocked with 5%BSA for one hour at R.T. For
474 primary antibody incubation, α-ZIP9 antibody [(SLC39A9 Antibody (PA5-52485),
475 Thermofisher Scientific, Waltham, MA)] was diluted 1:500 in 1% BSA and cells were incubated
476 overnight at 4ºC. After washing three times with PBS on a shaker, the slide was incubated with
477 Biotinylated Secondary antibody (Vectastain Kit, Peroxidase Rabbit IgG, PK-4001) for one hour
478 at R.T. Cells were washed three times with PBS, ABC reagent (prepared 30 minutes in advance)
479 was added and samples were incubated for 30 minutes at R.T. After three washes with PBS,
480 samples were incubated for 1.5 minutes with Vector Laboratories DAB Peroxidase (HRP)
481 Substrate Kit (NC9276270. Vector laboratories, Burlingame, CA). Cells were counterstain with
482 hematoxylin (10 seconds, R.T.) (GHS316. Sigma-Aldrich) and mounted with SecureMount
483 (Fisher HealthCare™ PROTOCOL™ Mounting Media. #022-208. Fisher Scientific.
484 Thermofisher Scientific).

485

486 **Cell membrane labeling with testosterone-BSA-FITC**

487 WM46 were seeded over coverslips in p12-well culture plate, after 24 hours cells TU2% media
488 was removed, and cells were grown in Serum-free TU media for 24 hours. Cells were treated
489 with APA (8mM) or DMSO as vehicle control. After one hour, cells were treated with 0.25µM
490 testosterone 3-(O-carboxymethyl) oxime:BSA-fluorescein isothiocyanate (T-BSA-FITC)

491 conjugate (T5771, Sigma-Aldrich, Munich, Germany) diluted in Tris-Buffer (pH 7.2) for 20 min
492 at room temperature. Negative control cells were incubated with 0.25 μM BSA-FITC (A9771,
493 Sigma-Aldrich, Munich, Germany) diluted in Tris-Buffer (pH 7.2) for 20 min at room
494 temperature. The medium was then aspirated, and cells were fixed for 7 minutes with 4%PFA.
495 Cells were washed three times with PBS (5 minutes each) and mounted with ProLong Gold
496 antifade reagent with DAPI (#P36935; Thermo Fisher Scientific). Images were captured using a
497 Leica DM IL microscope and registered using LAS software.
498
499 **Quantitative RT-PCR**
500 RNA was extracted using RNeasy kit (Qiagen. #74104) following the manufacturer's
501 instructions. cDNA was obtained using High Capacity cDNA Reverse Transcription Kit
502 (Applied Biosystems #4368814). For quantitative real-time PCR, PowerUP™ SYBR™ Green
503 Master Mix (Applied Biosystems #A25741) was used. ViiA 7 Real-Time PCR System was used
504 to perform the reaction (Applied Biosystems). Values were corrected by β-actin expression. The
505 $2^{-\Delta\Delta Ct}$ method was applied to calculate the relative gene expression. Primers used for the
506 amplification are included in Table S2.
507
508 **Mice, subcutaneous tumors and pharmacologic treatments**
509 All mice were purchased from Taconic Biosciences, Inc. (Rensselaer, NY, USA). 8- to 10-week
510 old male and female C57BL/6NTac or IcrTac:ICR-Prkdcscid mice were allowed to reach
511 sexually mature ages or to acclimatize for one week prior to being used in experiments. These
512 studies were performed without inclusion/exclusion criteria or blinding but included
513 randomization. Based on a two-fold anticipated effect, we performed experiments with at least 5

514 biological replicates. All procedures were performed in accordance with International Animal
515 Care and Use Committee (IACUC)-approved protocols at the University of Pennsylvania.
516 Subcutaneous tumors were initiated by injecting tumor cells in 50% Matrigel (Corning, Bedford,
517 MA, USA) into the subcutaneous space on the right flanks of mice. 10 x 10^6 human WM46 or 10
518 x 10^5 murine YUMM1.7 cells were used for each tumor. Oral administration of vehicle,
519 bicalutamide (30mg/kg/day) or apalutamide (20mg/kg/day) was performed daily. 100µl of drug
520 was administrated by oral gavage [10%DMSO:90%Vehicle (15% ethanol:85% sesame oil)].
521 Weight and health status of the mice as well as tumor growth were monitored daily. As
522 subcutaneous tumors grew in mice, perpendicular tumor diameters were measured using calipers.
523 Volume was calculated using the formula $L \times W^2 \times 0.52$, where L is the longest dimension and
524 W is the perpendicular dimension. Animals were euthanized when tumors exceeded a protocol-
525 specified size of 15 mm in the longest dimension. Secondary endpoints include severe ulceration,
526 death, and any other condition that falls within the IACUC guidelines for Rodent Tumor and
527 Cancer Models at the University of Pennsylvania.
528
529 **Statistical analysis**
530 For experiments comparing two groups (treated vs control), significance was calculated using the
531 Mann-Whitney test. For experiments with more than two groups, one-way ANOVA with
532 Tukey's honest significance difference test was performed. For the tumor growth studies *in vivo*,
533 non-linear regression analysis was performed to get the Exponential Growth Equation and
534 doubling times for tumor growth. To analyze the slopes of the curves and to compare them
535 between groups, linear regression analysis was performed. All the statistical analyses in this
536 work were performed using Graphpad Prism Software. Error bars represent standard error of the

537 mean (SEM). **** p value≤0.0001; *** p value≤0.001; ** p value≤0.01; * p value≤0.05;
538 n.s>0.05.
539
540 **Acknowledgements**
541 The authors thank the University of Pennsylvania Skin Biology and Disease Research-based
542 center for analysis of tissue sections and University of Pennsylvania Pathology Clinical Service
543 Center—Anatomic Pathology Division for the AR staining of the tissue microarray. **Funding:**
544 T.W.R. is supported by grant from the NIH/NCI (R01 CA163566, R41CA228695), and by the
545 Stiefel award from the Dermatology Foundation. This work was also supported in part by the
546 Penn Skin Biology and Diseases Resource-based Center (P30-AR069589), the Melanoma
547 Research Foundation to T.W.R., and R37 GM56328 to J.K.F**. Author Contributions:** C.A.P.,
548 R.P., A.T. performed the experiments. C.A.P., R.P. and J.K.F designed and performed the
549 experiments to study zinc influx. J.K.F provided experimental material and reviewed the
550 manuscript. J.T.S, scored the tissue microarray and reviewed the manuscript. C.A.P, C.A.N. and
551 T.W.R designed experiments and wrote the article. **Competing interests:** C.A.P., C.A.N., and
552 T.W.R., and are inventors on a provisional patent held by the University of Pennsylvania related
553 to this work.
554
555
556
557
558
559

560 **Figure legends**

561 **Fig. 1: Biologic sex and testosterone promote proliferation of melanoma models lacking**
562 **detectable AR.** Tumor growth of human WM46 melanoma in male and female immunodeficient
563 SCID mice. Tumor doubling times are 16.2 and 18.6 days for males and females respectively
564 (Non-linear regression analysis/Exponential fit. See also Sup. Fig. 1 for expanded statistical
565 analysis). **B.** Cell proliferation (cell number) determined after 6 days of treatment with vehicle
566 (DMSO), 100nM testosterone (T) or 100nM dihydrotestosterone (DHT). Human primary
567 melanocytes (H.Mel.) and human melanoma WM46 cells are shown. Graphs represent the
568 average of three independent experiments. **C.** Cell proliferation of human WM46 and murine
569 YUMM1.7 melanoma cells exposed to increasing concentrations of testosterone (T) (left panels)
570 or dihydrotestosterone (DHT) (right panel). **D.** AR mRNA expression in a battery of human
571 melanoma lines, and murine YUMM1.7 determined by qPCR. Two human prostate cancer lines
572 were used as a positive control (VCaP and LNCaP). **E.** AR protein expression determined by
573 Western blot with two different antibodies. Upper line = Androgen Receptor [(D6F11) XP®
574 Rabbit mAb #5153. Lower line = Recombinant Anti-Androgen Receptor antibody [EPR1535(2)]
575 (ab133273). β-actin was used as loading control.
576 ** p value≤0.01; * p value≤0.05.
577

578 **Fig 2: ZIP9 is active in human melanoma cells, and is broadly expressed in human**
579 **melanocytic tumors. A.** ZIP9 protein expression determined by western blot in primary
580 melanocytes and a battery of human melanoma cell lines. **B.** Time-lapse *in vivo* analysis of Zn^{++}
581 influx in WM46 cells upon testosterone addition (100nM). FluoZin-3 was used as Zn^{++} reporter.
582 **C.** Intracellular levels of Zn^{++} after long-term testosterone treatment (96 hours; 100nM
583 testosterone). Zinc levels were measured as fluorescence intensity per cell. FluoZin-3 was used

584 as Zn^{++} reporter. Representative images are shown on the right at indicated time-points. **D.**
585 WM46 relative proliferation (cell number) after 6 days in the presence of 100 nM testosterone
586 (T) +/- 200 nM zinc chelator (TPEN). **E.** WM46 proliferation in the presence exogenous divalent
587 cations Zn^{++} Fe^{++} and Mn^{++}. Cells were grown for 6 days and treated as indicated in the legend.
588 Error bars represent standard error of the mean (SEM). **F.** Validation of ZIP9 [(SLC39A9
589 Antibody (PA5-52485)] and androgen receptor [(Leica AR-318-L-CE, clone AR27 (clone AR27,
590 1:25)] antibodies for immunohistochemistry. ZIP9 staining performed in wild-type and ZIP9
591 knock-out cells. Prostate gland tissue and human prostate cancer samples were used as positive
592 controls for AR. Representative images of human melanoma samples stained for ZIP9 and AR.
593 Tumors expressing low, medium and high levels of ZIP9 are shown. Replicates from the same
594 samples stained for AR are shown. 20X magnification (1.6X zoom). Scale bar=60μM. **G.**
595 Graphic representation of the % of tumors that express ZIP9. Data from nevus, primary
596 melanomas and metastatic melanoma are displayed. **H.** Graphic representation of the percentage
597 of nevi, primary lesions and metastatic tumors classified according to ZIP9 intensity (Score 1=1-
598 25%, 2=26-50%, 3=51-75%, 4=76-100%).
599 **** p value≤0.0001; ** p value≤0.01; * p value≤0.05; n.s>0.05.
600
601 **Fig. 3: ZIP9 mediates testosterone effects in melanoma. A.** Proliferation (cell number) of
602 isogenic clonal populations of WM46 wtZIP9 and ΔZIP9 cells exposed to increasing
603 concentrations of testosterone (T) and dihydrotestosterone (DHT). Two different guides were
604 used to generate two different knock-out clones (ΔZIP9). The graph represents the average of
605 three independent experiments. **B.** Intracellular levels of zinc in human melanoma ΔZIP9 cells
606 measured as relative fluorescence intensity of FluoZin-3. Graphs represent the average of three

607 independent experiments. **C.** Relative cell proliferation in the presence of 100nM testosterone
608 (T), zinc chelator (200nM TPEN) and $ZnCl_2$ (400nM). Cells were cultured for 6 days. The graph
609 represents the average of three independent experiments. **D.** WM46 derived subcutaneous tumor
610 growth in SCID male and female mice (wtZIP9 and ΔZIP9). Linear regression analysis was
611 performed to compare the slopes of the curves. Additional statistical analyses are included in Fig.
612 S4H and I. Error bars represent standard error of the mean (SEM).
613 **** p value≤0.0001; *** p value≤0.001; ** p value≤0.01; * p value≤0.05; n.s>0.05.
614 **Fig. 4: Testosterone driven increase in melanoma proliferation requires ZIP9 and**
615 **activation of MAPK and YAP1. A.** RPPA analysis displaying changes in protein expression in
616 WM46 human melanoma cells following exposure to 100 nM testosterone (T) for increasing
617 amounts of time. Down-regulated proteins are shown in green; red color corresponds to up-
618 regulated proteins and control proteins showing no fold-change when compared to vehicle-
619 treated cells are shown in blue. **B.** Relative proliferation (cell number) after exposure to
620 pharmacologic ERK1/2 inhibition via 50nM RVD-523 (Ei) alone or in combination with
621 testosterone. wtZIP9 and ΔZIP9 WM46 cells are shown. The western blot shows levels of
622 phosphorylation of the ERK target RSK in wtZIP9 and ΔZIP9 WM46 cells (Ei represents RVD-
623 523). **C.** Western blot for YAP1 in fractionated WM46 lysates. Cells were treated with 100 nM
624 testosterone for the indicated times. β-Actin is used as cytoplasmic fraction positive control.
625 PARP is used as nuclear fraction positive control. **D.** Quantification of YAP-1 nuclear
626 immunodetection after 30 minutes of exposure to 100 nM testosterone (T) and/or 8μM
627 dobutamine (Dob) in wtZIP9 and ΔZIP9 cells. **E.** Proliferation of wtZIP9 and ΔZIP9 WM46
628 cells after treatment with 100nM testosterone (T) and/or the YAP inhibitor dobutamine (Dob). **F.**

629 Relative mRNA expression of YAP1 target genes after 30 minutes in the presence of 100 nM
630 testosterone and/or 8μM dobutamine. Error bars represent standard error of the mean (SEM).
631 *** p value≤0.001; ** p value≤0.01; * p value≤0.05; n.s>0.05.
632
633 **Fig. 5: Pharmacologic ZIP9 blockade inhibits melanoma *in vivo*. A.** Proliferation of human
634 melanoma cells (WM46) in the presence of 100 nM testosterone (T) +/- 2 μM AR inhibitors
635 (BIC:Bicalutamide; ENZ:Enzalutamide; APA:Apalutamide). Western blot showing ERK and p-
636 ERK proteins in WM46 cells treated with 100nM testosterone +/- 2μM BIC +/- 200 nM zinc
637 chelator (TPEN). **B.** Cell proliferation in human and murine derived melanoma cells (SK-MEL-
638 3, SK-MEL-2 and YUMM1.7) treated with 100 nM testosterone (T) in combination with
639 apalutamide (2 μM) (APA). **C.** Cell membrane labeling with cell impermeable testosterone-BSA
640 conjugated with FITC (0.25 μM). BSA-FITC (0.25 μM) was used as a negative control for
641 unspecific binding. Quantification of membrane labeling with T-BSA or the control BSA. The
642 graph represents the fluorescence intensity relative to the total area of each cell. **D.** Proliferation
643 of WM46 wtZIP9 and ΔZIP9 treated with 100 nM testosterone (T) in combination with
644 apalutamide (2 μM) (APA). **E.** Tumor growth and survival analysis in SCID male mice bearing
645 WM46 derived subcutaneous tumors (APA treatment: 20 mg/kg/day via oral gavage). ** p-
646 value<0.005 by ANOVA. Doubling time (non-linear regression analysis): Vehicle=11.11 days;
647 APA=25.22 days. **F.** Working model: ZIP9 activation promotes ERK phosphorylation and
648 induces YAP1 nuclear translocation. AR inhibitors [represented in the figure by apalutamide
649 (APA)] block testosterone effects through ZIP9 inactivation.
650 **** p value≤0.0001; *** p value≤0.001; ** p value≤0.01; * p value≤0.05; n.s>0.05.
651

652 **Figures**

Figure 1

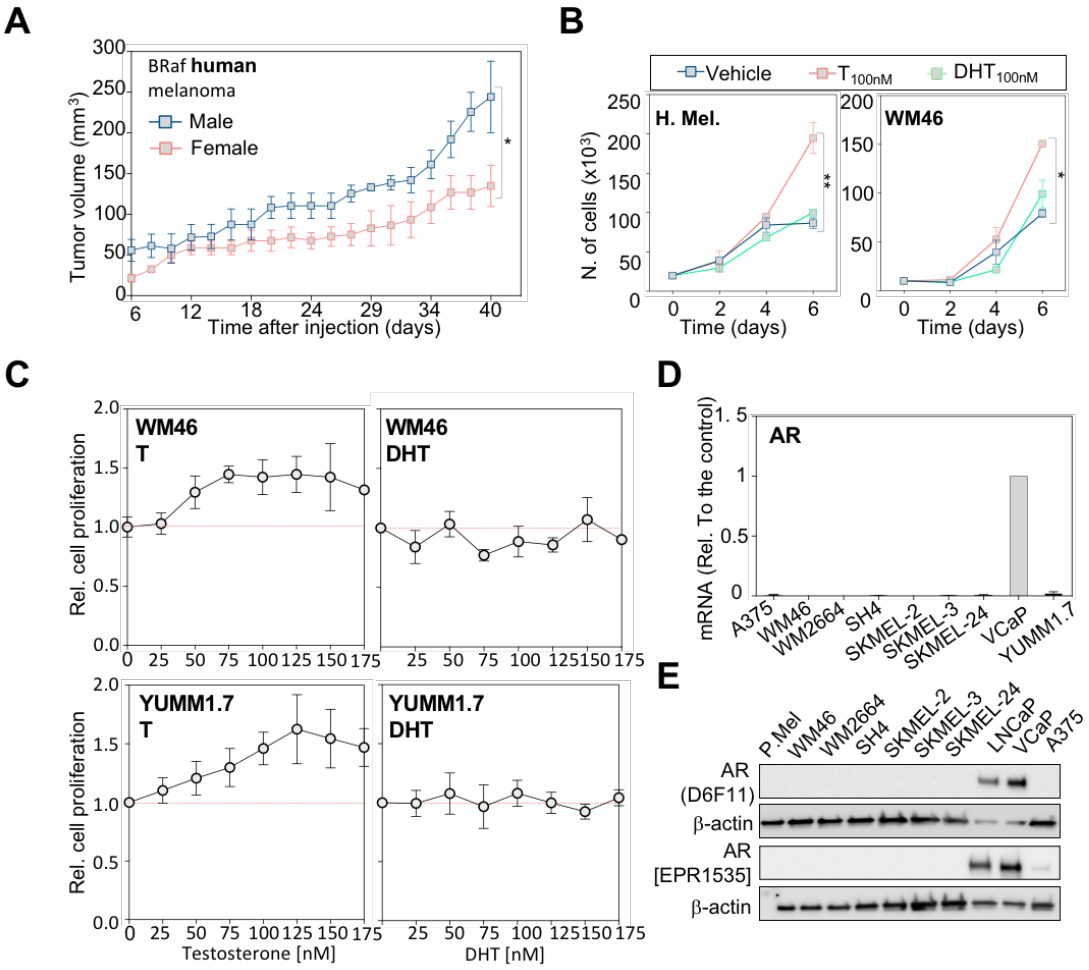

653

Figure 2

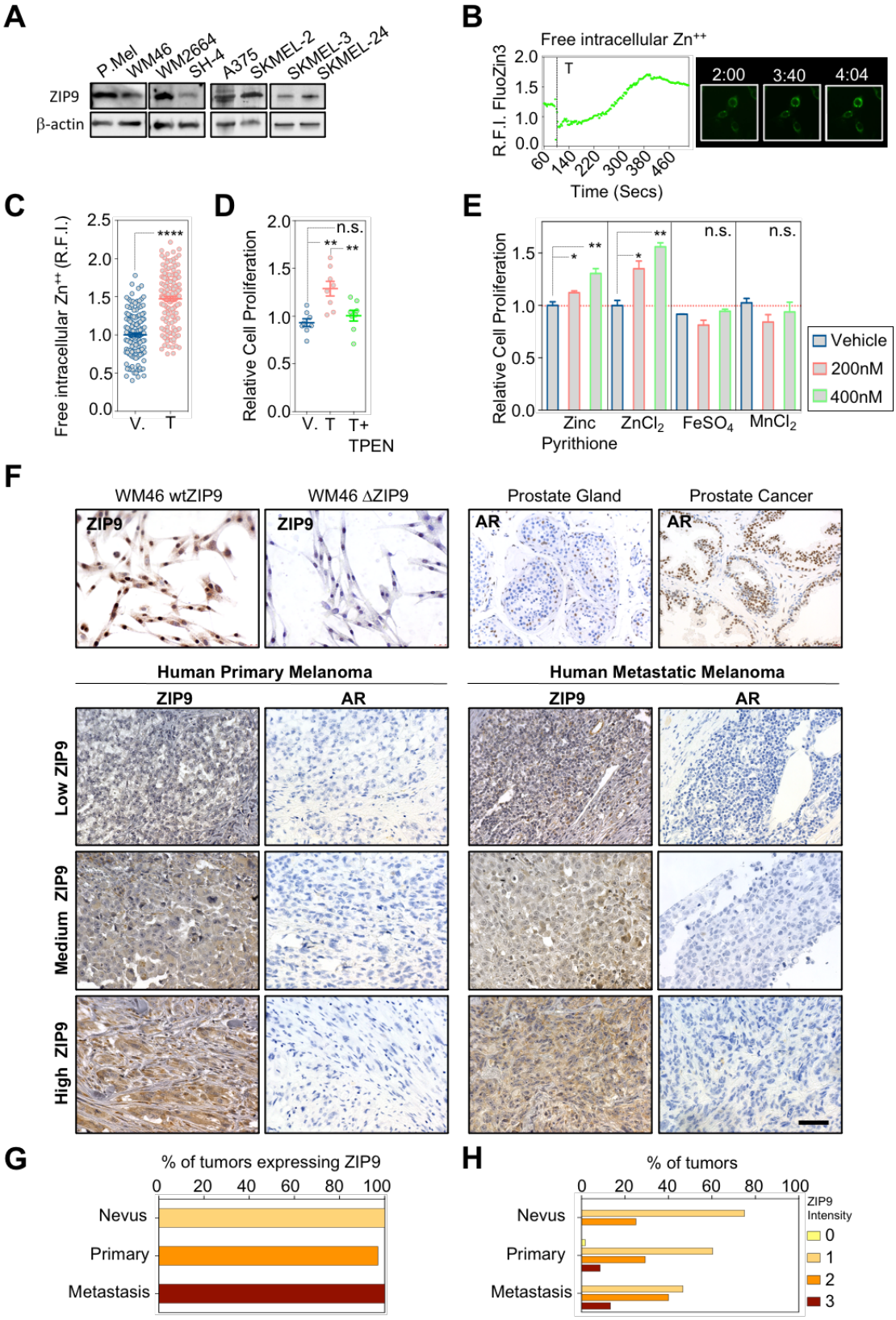
A
P.Mel
WM46
WM2664
SH-4
A375
SKMEL-2
SKMEL-3
SKMEL-24
ZIP9
β-actin
B
Free intracellular Zn++
R.F.I. FluoZin3
T
2:00
3:40
4:04
Time (Secs)
C
Free intracellular Zn++ (R.F.I.)
****
V.
T
D
Relative Cell Proliferation
n.s.
**
V.
T
T+ TPEN
E
Relative Cell Proliferation
Zinc Pyrithione
ZnCl2
FeSO4
MnCl2
Vehicle
200nM
400nM
F
WM46 wtZIP9
WM46 ΔZIP9
Prostate Gland
Prostate Cancer
ZIP9
AR
Human Primary Melanoma
Human Metastatic Melanoma
Low ZIP9
Medium ZIP9
High ZIP9
G
% of tumors expressing ZIP9
Nevus
Primary
Metastasis
H
% of tumors
ZIP9 Intensity
0
1
2
3

654

Figure 3

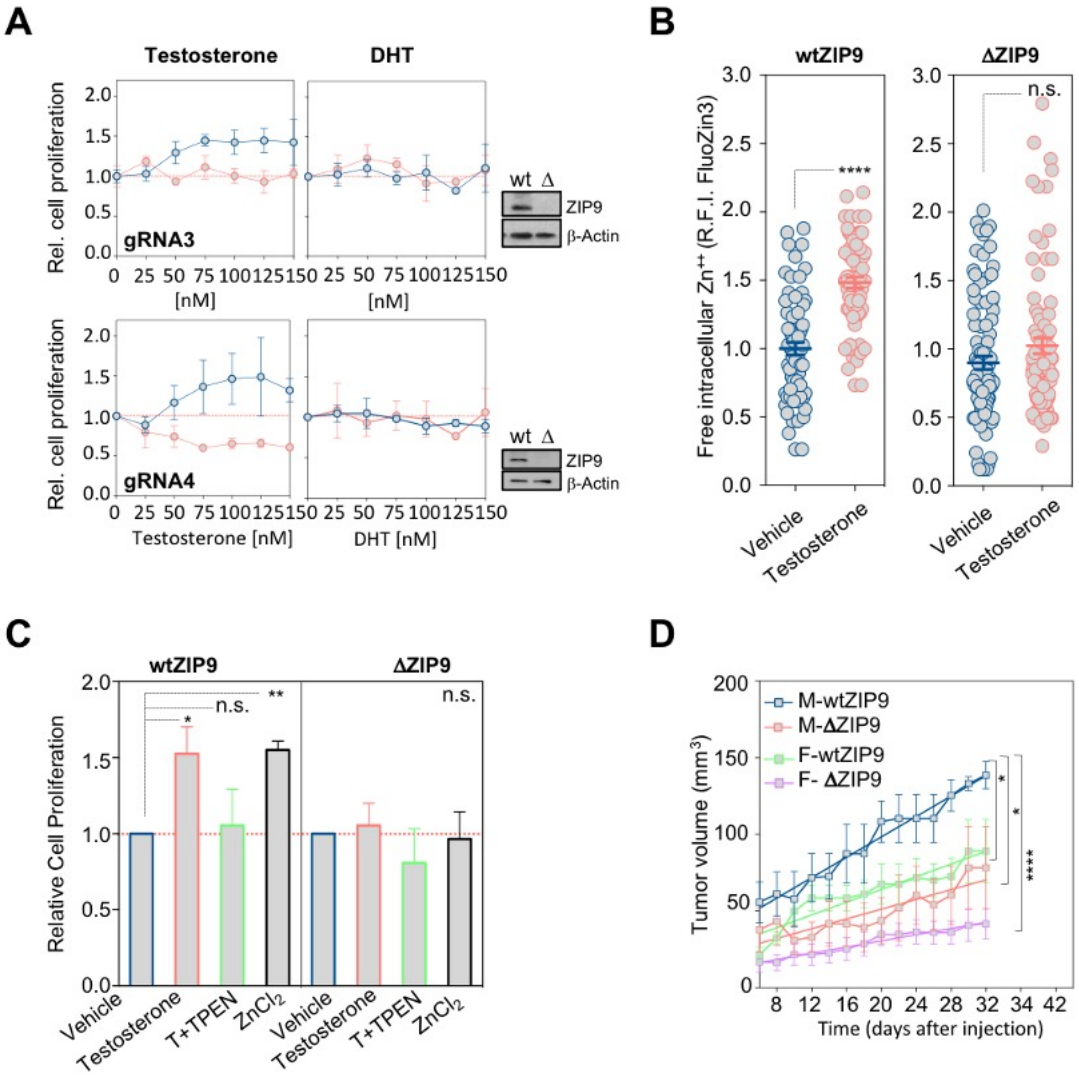
A
Testosterone
DHT
Rel. cell proliferation
gRNA3
gRNA4
[nM]
Testosterone [nM]
DHT [nM]
wt Δ
ZIP9
β-Actin
B
wtZIP9
ΔZIP9
Free intracellular Zn++ (R.F.I. FluoZin3)
****
n.s.
Vehicle
Testosterone
C
wtZIP9
ΔZIP9
Relative Cell Proliferation
n.s.
**
*
Vehicle
Testosterone
T+TPEN
ZnCl2
D
M-wtZIP9
M-ΔZIP9
F-wtZIP9
F- ΔZIP9
Tumor volume (mm3)
Time (days after injection)
*
*
****

Figure 4

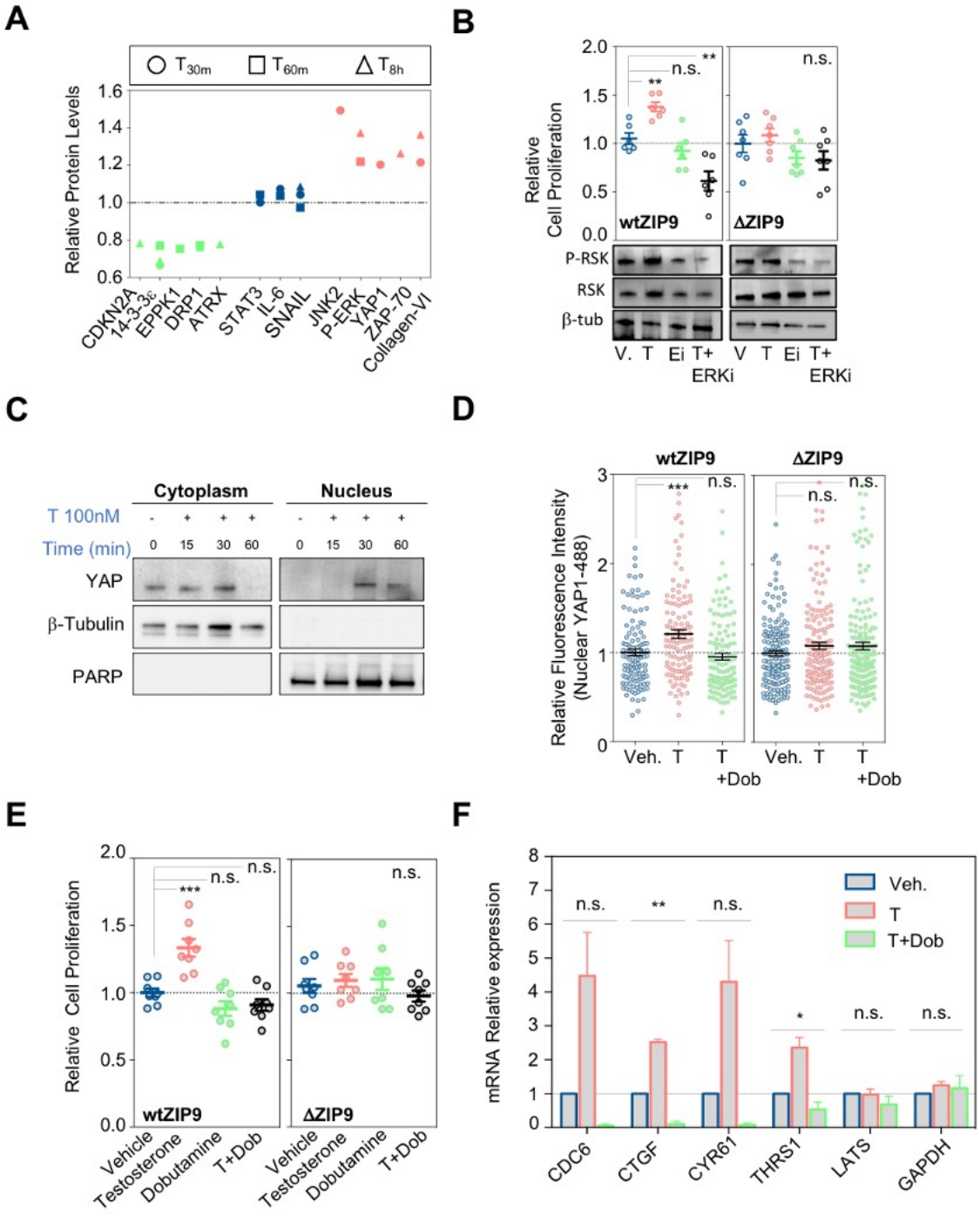

660

661

662

Figure 5

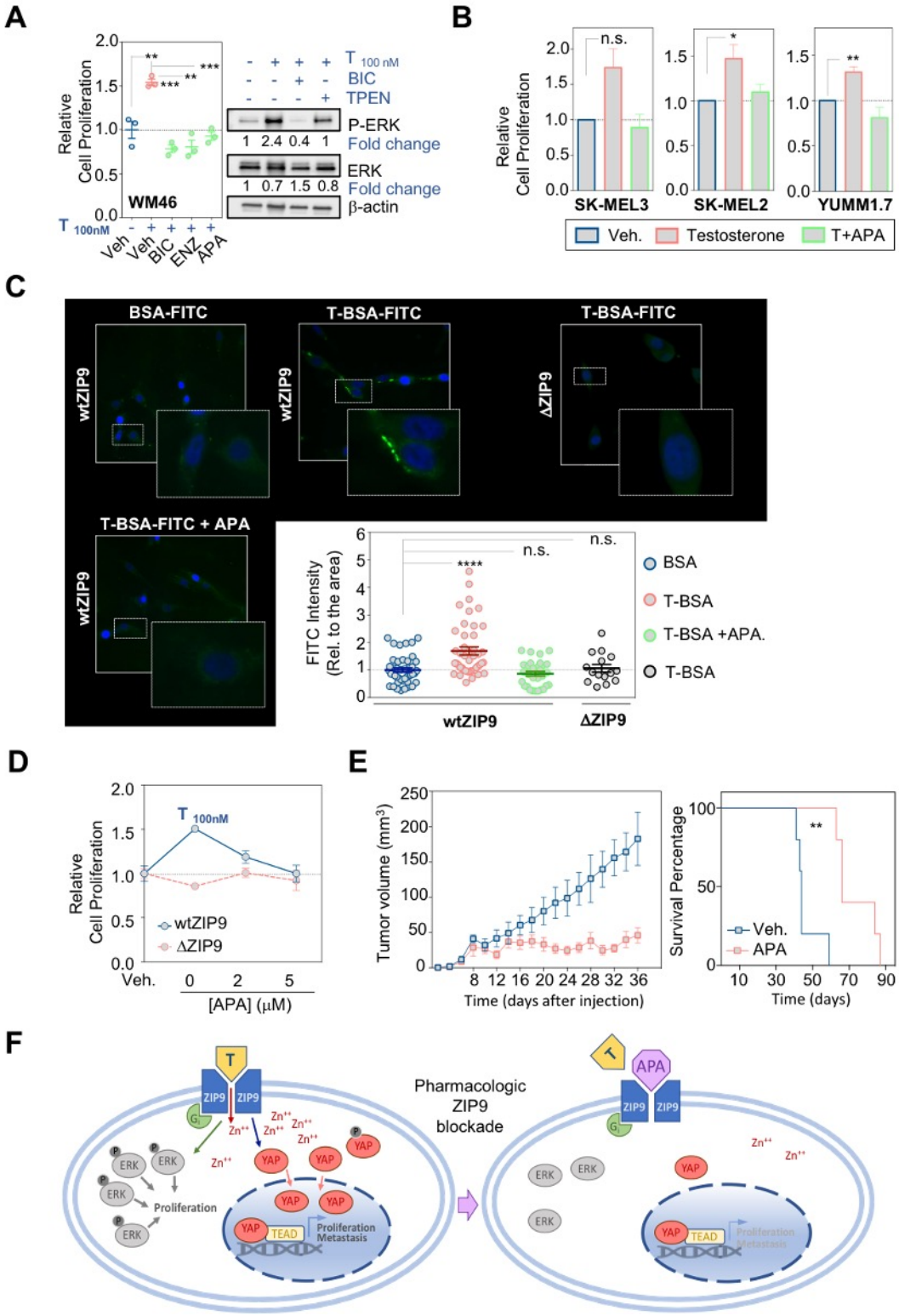
A
Relative Cell Proliferation
WM46
T 100nM
Veh
Veh
BIC
ENZ
APA
T 100 nM
BIC
TPEN
P-ERK
Fold change
1 2.4 0.4 1
ERK
1 0.7 1.5 0.8
β-actin
B
n.s.
SK-MEL3
SK-MEL2
YUMM1.7
Veh.
Testosterone
T+APA
C
BSA-FITC
T-BSA-FITC
T-BSA-FITC
T-BSA-FITC + APA
wtZIP9
ΔZIP9
FITC Intensity (Rel. to the area)
BSA
T-BSA
T-BSA +APA.
T-BSA
D
T 100nM
wtZIP9
ΔZIP9
[APA] (μM)
E
Tumor volume (mm³)
Time (days after injection)
Survival Percentage
Veh.
APA
Time (days)
F
Pharmacologic ZIP9 blockade
ZIP9
APA
ERK
YAP
TEAD
Proliferation
Metastasis

892 **References**

893

894 1. Siegel, R. L., Miller, K. D. & Jemal, A. Cancer statistics, 2020. *CA Cancer J Clin* **70**, 7–
895 30 (2020).
896 2. GLOBOCAN2018. https://bit.ly/2Vd3C6a.
897 3. Clemmesen, J. & Busk, T. Cancer Mortality Among Males and Females in Denmark,
898 England, and Switzerland: V. Incidence of Accessible and Inaccessible Cancers in Danish Towns
899 and Rural Areas. *Cancer Res* **9**, 415–421 (1949).
900 4. Hieken, T. J. *et al.* Sex-Based Differences in Melanoma Survival in a Contemporary
901 Patient Cohort. *Journal of Women's Health* (2020) doi:10.1089/jwh.2019.7851.
902 5. GLOBOCAN2018. Sex disparities in melanoma survival over time. shorturl.at/bkAI6.
903 6. Natale, C. A. *et al.* Activation of G protein-coupled estrogen receptor signaling inhibits
904 melanoma and improves response to immune checkpoint blockade. *Elife* **7**, (2018).
905 7. Natale, C. A. *et al.* Sex steroids regulate skin pigmentation through nonclassical
906 membrane-bound receptors. *Elife* **5**, (2016).
907 8. Sperling, M. A. *Pediatric Endocrinology-Mean Sex Steriod Concentration in Infants,*
908 *Children and adults.* (Elsevier Health Sciences, 2014).
909 9. Barbosa-Desongles, A., Hernández, C., Simó, R. & Selva, D. M. Testosterone induces
910 cell proliferation and cell cycle gene overexpression in human visceral preadipocytes. *Am. J.*
911 *Physiol., Cell Physiol.* **305**, C355-359 (2013).
912 10. Fu, R. *et al.* Novel evidence that testosterone promotes cell proliferation and
913 differentiation via G protein-coupled receptors in the rat L6 skeletal muscle myoblast cell line. *J.*
914 *Cell. Physiol.* **227**, 98–107 (2012).
915 11. Rodríguez-Lozano, D. C., Piña-Medina, A. G., Hansberg-Pastor, V., Bello-Alvarez, C. &
916 Camacho-Arroyo, I. Testosterone Promotes Glioblastoma Cell Proliferation, Migration, and
917 Invasion Through Androgen Receptor Activation. *Front. Endocrinol.* **10**, (2019).
918 12. Maasberg, M. *et al.* Androgen receptors, androgen-dependent proliferation, and 5 alpha-
919 reductase activity of small-cell lung cancer cell lines. *Int. J. Cancer* **43**, 685–691 (1989).
920 13. Allil, P. A. A., Visconti, M. A. & Isoldi, A. M. L. C. and M. C. Photoperiod and
921 Testosterone Modulate Growth and Melanogenesis of S91 Murine Melanoma. *Medicinal*
922 *Chemistry* http://www.eurekaselect.com/82341/article (2008).
923 14. Meeth, K., Wang, J. X., Micevic, G., Damsky, W. & Bosenberg, M. W. The YUMM
924 lines: a series of congenic mouse melanoma cell lines with defined genetic alterations. *Pigment*
925 *Cell Melanoma Res* **29**, 590–597 (2016).
926 15. Gao, W., Bohl, C. E. & Dalton, J. T. Chemistry and Structural Biology of Androgen
927 Receptor. *Chem Rev* **105**, 3352–3370 (2005).
928 16. Askew, E. B., Gampe, R. T., Stanley, T. B., Faggart, J. L. & Wilson, E. M. Modulation of
929 Androgen Receptor Activation Function 2 by Testosterone and Dihydrotestosterone. *J. Biol.*
930 *Chem.* **282**, 25801–25816 (2007).
931 17. Berg, A. H., Rice, C. D., Rahman, M. S., Dong, J. & Thomas, P. Identification and
932 characterization of membrane androgen receptors in the ZIP9 zinc transporter subfamily: I.
933 Discovery in female atlantic croaker and evidence ZIP9 mediates testosterone-induced apoptosis
934 of ovarian follicle cells. *Endocrinology* **155**, 4237–4249 (2014).
935 18. Matsuura, W. *et al.* SLC39A9 (ZIP9) regulates zinc homeostasis in the secretory
936 pathway: characterization of the ZIP subfamily I protein in vertebrate cells. *Biosci. Biotechnol.*
937 *Biochem.* **73**, 1142–1148 (2009).

938 19. Fatfat, M. *et al.* Copper chelation selectively kills colon cancer cells through redox
939 cycling and generation of reactive oxygen species. *BMC Cancer* **14**, 527 (2014).
940 20. He, L. *et al.* ZIP8, member of the solute-carrier-39 (SLC39) metal-transporter family:
941 characterization of transporter properties. *Mol. Pharmacol.* **70**, 171–180 (2006).
942 21. Leal, M. F. *et al.* Clinical implication of 14-3-3 epsilon expression in gastric cancer.
943 *World J. Gastroenterol.* **18**, 1531–1537 (2012).
944 22. Ruas, M. & Peters, G. The p16INK4a/CDKN2A tumor suppressor and its relatives.
945 *Biochim. Biophys. Acta* **1378**, F115-177 (1998).
946 23. Germann, U. A. *et al.* Targeting the MAPK Signaling Pathway in Cancer: Promising
947 Preclinical Activity with the Novel Selective ERK1/2 Inhibitor BVD-523 (Ulixertinib). *Mol.*
948 *Cancer Ther.* **16**, 2351–2363 (2017).
949 24. Han, Y. Analysis of the role of the Hippo pathway in cancer. *Journal of Translational*
950 *Medicine* **17**, 116 (2019).
951 25. Zhao, B., Li, L., Tumaneng, K., Wang, C.-Y. & Guan, K.-L. A coordinated
952 phosphorylation by Lats and CK1 regulates YAP stability through SCFβ-TRCP. *Genes Dev* **24**,
953 72–85 (2010).
954 26. Fujii, M. Exploration of a new drug that targets YAP. *J. Biochem.* **152**, 209–211 (2012).
955 27. Bulldan, A., Malviya, V. N., Upmanyu, N., Konrad, L. & Scheiner-Bobis, G.
956 Testosterone/bicalutamide antagonism at the predicted extracellular androgen binding site of
957 ZIP9. *Biochim Biophys Acta Mol Cell Res* **1864**, 2402–2414 (2017).
958 28. Ponnusamy, S. *et al.* Orally-Bioavailable Androgen Receptor Degrader, A Potential
959 Next-Generation Therapeutic for Enzalutamide-Resistant Prostate Cancer. *Clin. Cancer Res.*
960 (2019) doi:10.1158/1078-0432.CCR-19-1458.
961 29. Chi, K. N. *et al.* Apalutamide for Metastatic, Castration-Sensitive Prostate Cancer. *N.*
962 *Engl. J. Med.* **381**, 13–24 (2019).
963 30. Kayigil, O., Atahan, O. & Metin, A. Cyproterone acetate monotherapy in advanced
964 prostatic carcinoma. *Int Urol Nephrol* **29**, 213–220 (1997).
965 31. Thomas, P., Pang, Y. & Dong, J. Membrane androgen receptor characteristics of human
966 ZIP9 (SLC39A) zinc transporter in prostate cancer cells: Androgen-specific activation and
967 involvement of an inhibitory G protein in zinc and MAP kinase signaling. *Mol. Cell. Endocrinol.*
968 **447**, 23–34 (2017).
969 32. Thomas, P., Pang, Y., Dong, J. & Berg, A. H. Identification and Characterization of
970 Membrane Androgen Receptors in the ZIP9 Zinc Transporter Subfamily: II. Role of Human
971 ZIP9 in Testosterone-Induced Prostate and Breast Cancer Cell Apoptosis. *Endocrinology* **155**,
972 4250–4265 (2014).
973 33. Fukada, T. & Kambe, T. Molecular and genetic features of zinc transporters in
974 physiology and pathogenesis. *Metallomics* **3**, 662–674 (2011).
975 34. Costello, L. C., Liu, Y., Zou, J. & Franklin, R. B. Evidence for a zinc uptake transporter
976 in human prostate cancer cells which is regulated by prolactin and testosterone. *J Biol Chem* **274**,
977 17499–17504 (1999).
978 35. Bafaro, E., Liu, Y., Xu, Y. & Dempski, R. E. The emerging role of zinc transporters in
979 cellular homeostasis and cancer. *Signal Transduction and Targeted Therapy* **2**, 1–12 (2017).
980 36. Ma, M. *et al.* Sustained androgen receptor signaling is a determinant of melanoma cell
981 growth potential and tumorigenesis. *J Exp Med* **218**, (2021).
982 37. Klein, S. L. & Flanagan, K. L. Sex differences in immune responses. *Nat. Rev. Immunol.*
983 **16**, 626–638 (2016).